Article

Performance of Cooperative Relay NOMA with Large Antenna Transmitters

Samuel Tweneboah-Koduah [1,*], Emmanuel Ampoma Affum [2], Kwame Agyemang-Prempeh Agyekum [2], Sunday Adeola Ajagbe [3,4] and Matthew O. Adigun [4]

[1] Department of Computer and Electrical Engineering, University of Energy and Natural Resources, P. O. Box 214, Sunyani, Ghana
[2] Department of Telecommunication Engineering, Kwame Nkrumah University of Science and Technology, PMB, Kumasi, Ghana
[3] Department of Computer Engineering, Ladoke Akintola University of Technology, 210214, Ogbomoso, Nigeria
[4] Department of Computer Science, University of Zululand, Kwadlangezwa 3886, South Africa
* Correspondence: samuel.tweneboah-koduah@uenr.edu.gh; Tel.: +233-240-987-199

Abstract: The potential of the Non-Orthogonal Multiple Access (NOMA) approach for wireless communications in the fifth generation (5G) and beyond can not be underestimated. This is because users with favorable channel conditions can serve as relays to improve system performance by employing Successive Interference Cancellation (SIC). Lately, the combination of NOMA and the cooperative relay has attracted the interest of researchers. The analysis of cooperative relay NOMA (CR-NOMA) with a massive multiple-input multiple-output (mMIMO) system is mainly based on theoretical channel models such as the correlated-based stochastic channel model (CBSM) even though the geometric-based stochastic channel model (GBSM) has been found to provide better, practical and realistic channel properties. This, in our view, is due to computational challenges. Again, the performance of CR-NOMA systems using the GBSM channel model with large antenna transmitters and network coding schemes has attracted little attention in academia. Therefore, the need to study mMIMO CR-NOMA that considers channel properties such as path-loss, delay profile and tilt angle has become vital. Furthermore, the co-existing of large antenna transmitters with coding schemes needs further investigation. In this paper, we study the performance of a two-stage mMIMO CR-NOMA network where the transmitter is represented as a uniform rectangular array (URA) or cylindrical array (CA). The communication channel from the transmitter (TX) to the user equipment (UE) through a relay station (RS) is modeled with a 3GPP's three-dimensional (3D) GBSM mMIMO channel model. To improve the analytical tractability of 3D GBSM, we defined the antenna element location vectors using the physical dimension of the antenna array and incorporated them into the 3D channel model. Bit-error rates, achievable rates and outage probabilities (OP) are examined using amplify-and-forward (AF) and decode-and-forward (DF) coding schemes. Results obtained show with fixed power allocation and SNR of 20 dB, far or weak users can attain a high achievable rate using DF and URA. Again, from the results, the combination of AF and CA presents better outage probabilities. Finally, the results indicate that the performance difference between CBSM and GBSM is marginal, even though the proposed 3D GBSM channel model has a higher degree of random parameters and computational complexities.

Keywords: geometric-based stochastic model (GBSM); correlated-based stochastic model (CBSM); cooperative relay-noma (CR-NOMA); massive MIMO (mMIMO); network coding schemes

1. Introduction

The design of 5G is to fundamentally fulfil the emerging requirements of wireless communication, such as high spectral and energy efficiency, low latency, massive device connectivity, high data rate and ultrahigh reliability [1–3]. Therefore, this requires a multiple

access technology that meets the network capacity within the limited radio spectrum [4–6]. NOMA technique is considered for 5G networks to improve system performance, high reliability, increased system capacity and coverage area [7–9]. NOMA, unlike orthogonal multiple access (OMA), uses the same time, code and or radio frequency resources to provide services to multiple users. This is done by introducing controlled interference through non-orthogonal resource allocation [10]. Most importantly, it supports large numbers of connections and high-congestion transmission [11]. The basic operation of NOMA is to superimpose multiple signals at the transmitter in the power domain. As shown in Figure 1, at the Base Station (BS), data from various users are superimposed on top of one another over the same time/frequency/code resource block. The BS uses a power allocation generator to assign different power levels to each user within resource block. The superimposed signal, $s(t)$, is transmitted through a fading channel with additive white Gaussian noise (AGWN) to the receiving user equipment (UE). The Gaussian channel's output is the sum of the input signal and an independent identically distributed noise signal from a Gaussian distribution of variance N, that may be produced by the receiver electronics [12]. In addition, at the UE, NOMA employs interference cancellation (SIC) method to improve network performance, to minimize interference and separate multiplexed users [13]. In NOMA, the weak user treats a strong user's signals as noise and directly decodes its signal [14]. The strong user on the other hand uses SIC to detect and decode their signals [7]. Additionally, weak users receive more power than strong users due to interference and poorer channel gains [15]. This is intended to maximize weak user transmission rate, experience and fairness [14].
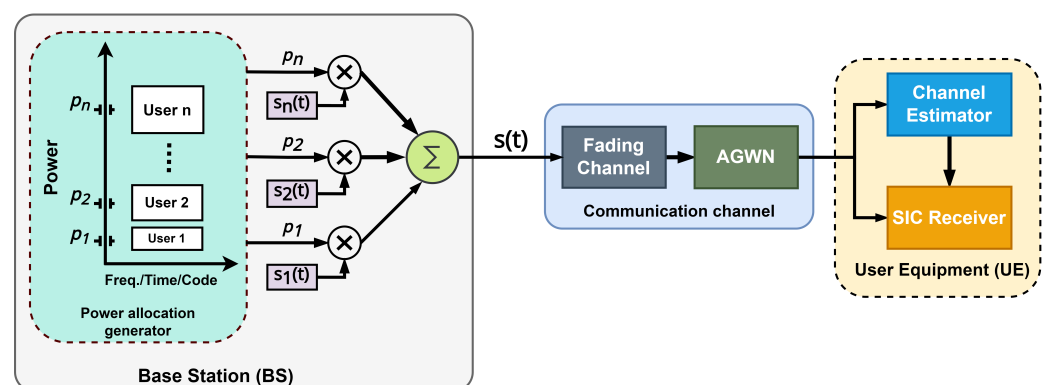
$p_1, p_2, ..., p_n$ = Power allocation coefficient of users

$s_1(t), s_2(t), ..., s_n(t)$ = Original signal of individual users

$s(t) = p_1 s_1(t) + p_2 s_2(t) + ... + p_n s_n(t)$ is the superimposed signals

Figure 1. NOMA system architecture for downlink communication.

The concept of CR-NOMA was established in [16] to increase the performance of cell edge users. In CR-NOMA several network coding schemes are introduced to secure the quality of service to weak users in the communication network [15]. This is to minimize interference and enhance performance. These schemes are decode-and-forward, compress-and-forward, amplify-and-forward, and compute-and-forward.

1.1. Review of Existing Works and Motivation

1.1.1. 5G Massive MIMO Channel Models

To assess the performance of 5G wireless communication systems, two types of channel models are commonly used; correlation-based stochastic models (CBSMs) and geometry-based stochastic models (GBSMs) [17,18]. The former has a lesser level of complexity and is mostly used to analyze the theoretical performance of MIMO systems [17,19].

However, the accuracy of a realistic MIMO system is restricted, and modeling wireless channels with nonstationary phenomena and spherical wave effects is challenging [17,19,20]. In contrast, GBSM has increased processing complexity, however, it can correctly represent

true channel parameters and is better appropriate for mMIMO channel models [17]. GBSM incorporates channel properties such as path-loss, delay profile, tilt angle, angle of arrivals, etc into the channel modeling for better performance evaluation [20–22].

1.1.2. Performance of CR-NOMA with CBSM Channel Model

The review of performance of CR-NOMA using AF/DF coding schemes is presented in this section. As previously stated, the performance of CR-NOMA has been extensively studied utilizing various network coding schemes and channel characteristics [23–27]. The use of a relay in NOMA system is to improve system performance and extend the network coverage [28]. The effect of various network coding schemes on the performance of CR-NOMA has been studied in [21,29]. In order to improve reliability, enhance the spectrum, power effectiveness and network connectivity, certain network terminals interact and aid one another by using the broadcast aspect of the wireless connections [30]. In CR-NOMA, users or devices with poor channel conditions, who often suffer from power losses at the cell edge, can be assisted by other users or devices with strong channel conditions by serving as transmission relays. This can greatly improve the reliability of the weak user's reception. There are two well-known network coding schemes: amplify-and-forward (AF) and decode-and-forward (DF) coding schemes [31,32]. The AF coding scheme relay simply amplifies and forwards a scaled version of its observation to the destination [23,33–36]. A CSI-assisted AF relay exploits instantaneous CSI of source-to-relay link to adjust its gain which has superior performance over the fixed gain AF relay has been studied in [37–42]. DF coding scheme relay, on the other hand, decodes the received signal first before re-transmitting the decoded signal to the destination [23]. Others such as compress-and-forward (CF) and computer-and-forward(CpF) have been studied in [15,40,43–49] respectively. With the CF approach, the signal is compressed and sent to the target location(s), whereas with the CpF however does not requires CSI and exploits signal couplings produced by the channel to remove noise noise and mitigate interference at the relays thereby reducing the number of relays required. Resource allocation optimization has been analyzed using the above coding schemes in [45,50–60] in order to improve CR-NOMA performance. Majority of the CR-NOMA performance evaluations (OP, achievable rate, BER, etc.) stated above have been limited to CBSM channel models. Table 1, presents a summary of CR-NOMA performance using CBSMs with AF/DF coding schemes. Figure 2 presents the CR-NOMA model that used and studied in the above studies, where the channel between the transmitter, relay and the users is modeled as CBSM. To improve system spectral efficiency and reduce challenges in channel state information (CSI) acquisition, CR-NOMA with MIMO and mMIMO have been studied in [47,61]. In [47], the authors considered the Saleh-Valenzuela millimeter-wave channel model for beamforming analysis, and no network coding schemes were considered. Again the analysis focused on user relay and not dedicated relay. The authors in [61], studied the application of relay to mMIMO NOMA. However, the analysis was based on CBSM. They proposed a general framework for a multiple-relay aided massive NOMA system. At the TX, the authors considered circular array for the analysis which is not a typical antenna array typologies for massive MIMO systems according to [17].

1.2. Motivation

From the above literature, the techniques and analysis that have been used to improve system performance of CR-NOMA have predominantly been restricted to only CBSM [62–76].
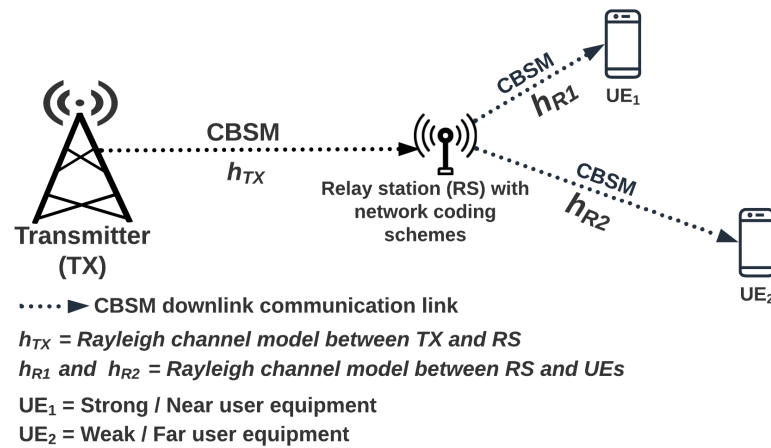
Figure 2. Downlink cooperative relay aided NOMA network with CBSM channel.

Table 1. Performance of AF/DF based CR-NOMA with CBSM channel model

Ref	Coding Scheme	Channel Model & Antenna Type	Transmission Mode	Performance Metrics	Outcome
[47]	DF relay	CBSM (Saleh-Valenzuela), multiple antenna	Downlink	Achievable sum rate	The spectrum and energy efficiency of beamspace MIMO are higher than those of conventional beamspace systems.
[61]	AF relay	CBSM (Rayleigh), multiple antenna	Downlink	Spectral efficiency	The number of BS antennas enhances system spectral efficiency.
[77]	DF relay	CBSM (Rayleigh), single antenna	Downlink	Diversity gain, outage probability	A two-stage relay with DF achieves maximum diversity gain while reducing outage probability.
[78]	AF relay	CBSM (Rayleigh), multiple antenna	Downlink	Outage probability	MIMO improves outage probabilities, but that depends on the relay location.
[79]	AF buffer-aided relay	CBSM (Rayleigh), single antenna	Downlink	Outage probability, throughput and diversity gain	Improve outage probability with increase buffer size. Incorporating channel-to-packet matching enhances system performance. Optimal selection of buffer size provides a significant delay.
[80]	DF relay	CBSM (Rician), single antenna	Downlink	Achievable rate	Gauss-Chebyshev interpolation is efficient to approximate achievable rate.
[81]	DF relay	CBSM (Rayleigh), single antenna	Downlink	Achievable sum rate	Configurable decoding achieves high sum rate even under strong inter-user interference and SNR.
[82]	DF relay	CBSM (Rayleigh), single antenna	Multi-relay Downlink	Outage probability and ergodic sum-rate	In comparison to typical NOMA and OMA systems, the ergodic sum rate and outage probability are enhanced.
[83]	DF relay	CBSM (Rayleigh), multiple antenna	Downlink	Outage probability and diversity order	A combination of antenna-and-relay selection strategies can provide optimal outage performance and diversity order that outperforms conventional systems.
[84]	DF relay	CBSM (Rayleigh), multiple antenna	Downlink	Secrecy outage probability	There is better outage performance of the system even in the presence of a jamming signal.
[85]	AF and DF relay	CBSM (Rayleigh), multiple antenna with energy harvesting (EH) capabilities	Downlink	Average sum-rate and secrecy rate	The position of the relay is crucial for maximum performance. To maximize the secrecy rate, the EH time duration must be carefully considered.

Table 1. *Cont.*

Ref	Coding Scheme	Channel Model & Antenna Type	Transmission Mode	Performance Metrics	Outcome
[86]	DF relay	CBSM (Rayleigh), single antenna with buffer capabilities	Downlink	Average throughput and outage probability	There is a significant improvement in system throughput at both low and high SNR bands, as well as diversity order with an increased number of relays.
[87]	DF relay	CBSM (Rayleigh), single antenna	Uplink	Weighted sum-rate maximization	The proposed cooperative NOMA approach outperforms both the non-cooperative NOMA benchmark and the traditional OMA in terms of attainable rate and throughput.
[88]	DF relay	CBSM (Rayleigh), single antenna	downlink	Ergodic sum-rate and outage probability	The proposed system provides better outage probability and superior ergodic sum rate over equivalent conventional systems.

CBSM is basically used for theoretical analysis and has less accuracy for real-world mMIMO systems due to the nonstationary phenomenon and spherical effects [17,89]. The best we can tell is that authors in [47] have analyzed CR-NOMA performance using GBSM based on Saleh-Valenzuela channel model. For mMIMO systems, there are several typical antenna array configurations. These include linear antenna array, rectangular antenna array, spherical antenna array, distributed antenna array and cylindrical antenna array [17]. With CR-NOMA, only linear antenna array has been examined so far in [61].

Based on the above, the motivation of this work is to address the missing gap in the literature on CR-NOMA concerning the adoption of 3GPP 3D GBSM channel model with large antenna transmitters such as URA and CA. Our research aims to provide solutions to the following research challenges to fulfill future demands of wireless communication systems: (1) What effect will the large antenna transmitters (CA or URA) modeling have on CR-NOMA system's performance? (2) How will mMIMO CR-NOMA work when the user, the dedicated relay, and transmitter all use the 3D GBSM channel model? (3) How will the coexistence of large antenna transmitters, 3D GBSM channel models, and coding schemes affect performance of CR-NOMA? (4) what coding scheme and large antenna combination will provide the superior performance when using the GBSM channel model for mMIMO CR-NOMA regarding outage probability, achievable rate, and bit-error-rate (BER)?

1.3. Contribution of the Work

We consider a two-stage downlink network system model with a dedicated relay. We use the 3GPP and WINNER+ models that follow the GBSM approach in [90–92] and provide a 3D GBSM channel model [93,94] when the transmitter is either URA or CA. We use the channel model in a CR-NOMA system where the transmitter's antenna is a massive antenna array system. We analyse the performance of the proposed system when the RS uses either AF or DF network coding scheme. The reason is that research in [21,95] shows that a significant component of energy is emitted in the elevation of the WINNER+ and 3GPP models. As a result, specifying propagation pathways in azimuth alone does not improve performance [95]. Furthermore, the WINNER+ and 3GPP models include the antenna boresight's elevation angle in the channel equation. We use URA and CA because their radiated MIMO signals can be adjusted in 3D space to boost system capacity [21]. Again, a massive antenna array can reduce clutter by using scanning acceleration and a space-time signal. Furthermore, it permits the creation of concentrated beams in any horizontal direction [21]. To reduce the computational complexity of the 3D GBSM channel model, we define the antenna element location vector using the physical dimension of the antenna array and incorporate it into the 3D channel model [21,96,97]. To enhance the performance of the proposed mMIMO CR-NOMA system, two coding schemes, AF and DF, are used with the channel model. The results present the performances of the

combination of coding schemes and large antenna transmitters regarding achievable rate, outage probability and Bit-error rate (BER).

Again, to fill the gap in the above literature on the CR-NOMA system concerning the adoption of 3GPP's 3D GBSM channel model with large antenna transmitters, this paper aims to assess the system usage performances using the proposed channel model. For clarity, the major contributions and objectives of the paper are:

i.   We examine a two-stage downlink mMIMO CR-NOMA GBSM system and introduce a new channel model when the transmitter is URA or CA. To reduce the computational complexity of the 3D GBSM channel, we define the antenna elements' location vector based on the physical dimension of the antenna array. We illustrate the transmitter with a massive antenna system following the models discussed in [17]. Here, the relay and user equipment only has a single antenna.

ii.   Two coding schemes, AF and DF, are incorporated into the channel model to improve the channel performance.

iii.   For performance analysis, evaluation and comparison, we present outage probability and achievable rate for the two-stage mMIMO CR-NOMA system.

iv.   Final findings show that the joint contribution between large antenna transmitters and coding schemes with 3D GBSM CR-NOMA presents possible advantages for future communications systems concerning achievable rate, outage probability and Bit-error rate (BER).

The paper is organized as follows. Section 2 presents the proposed system model for the 3D GBSM URA/CA channels for mMIMO CR-NOMA network. In Sections 3 and 4 respectively, we present the performance analysis, and simulation and numerical results of the system. We conclude the paper and provide future scope in Section 5.

2. System Model

This section describe a two-stage downlink (DL) communication system, where the transmitter (TX) sends messages to user equipment (UE) through a dedicated relay, as indicated in Figure 3. The TX has a large-scale antenna array (URA or CA) for high spectral-efficient massive access, whereas the UEs and relay station (RS) each have a single antenna. Unlike the CR-NOMA model in Figure 2, where the channel from TX to UEs through RS are theoretical channel models (CBSM), the proposed model replaces the CBSM channel in Figure 2 with GBSM channel model, as shown Figure 3. The strong user equipment (UE_1) in the proposed system of Figure 3 is near the RS, whereas the weak user equipment (UE_2) is farther away from the RS.
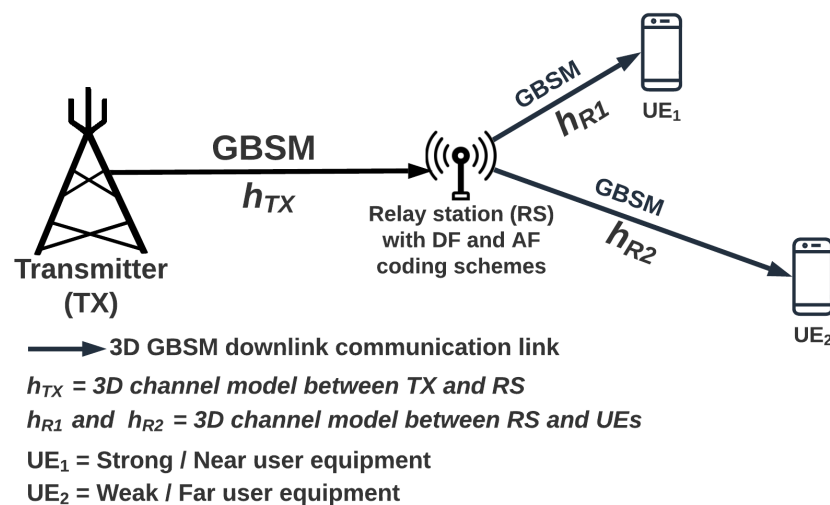

Figure 3. Proposed model of the downlink cooperative relay NOMA network with mMIMO.

The communication link from TX to UEs through RS is modeled using a 3D GBSM channel model with a single bounce and single cluster. In this context, URA and CA is considered as the transmitters. The proposed system uses two-time slots to achieve a seamless transmission from the TX to UEs through the RS. During the initial time slot, the TX sends signals to the relays using superposition coding. The combined signal ($\mathbf{x}$) of the two UEs with superposition coding is given by

$$\mathbf{x} = \sum_{i=1}^{2} \sqrt{\alpha_i P_s} s_i \tag{1}$$

where the ith user transmits power allocation factor, and the source signal is α_i and s_i, respectively. Noticeably, $\sum_{i=1}^{K} \alpha_i = 1 \leq P_s$ and $\mathbb{E}\|x_i\| \leq P_s$, where $K = 2$ user equipment and total transmit power is given as P_s.

Using NOMA concepts implies that power allocation factors are arranged according to users' proximity to the RS, that is $\alpha_1 < \alpha_2$ where α_1 and α_2 are the power allotment coefficient of the strong or near user equipment (UE_1) and the weak or far user equipment (UE_2) respectively. Hence, without loss of generality, the channel gains of the two UEs are arranged as $|\mathbf{h}_{R,1}|^2 \geq |\mathbf{h}_{R,2}|^2$. We exploit channel reciprocity through a conventional time division duplex mode [98]. We presume that MIMO downlink (DL) pilots with an N_t transmitting antenna allow the TX to estimate the DL channel. Generally, for a single-hop communication involving a transmitter and two users, the received signal (y) by the ith user at the destination with DL data transmission can be expressed as,

$$y_i = \mathbf{H}\mathbf{x} + n_i \tag{2}$$

where $\mathbf{x}$ is an $N_t \times 1$ data signal, $i = 1, 2$, $\mathbf{H}$ is the communication channel matrix such as the 3D channel realization matrix presented in (12) and (15), n_i is the additive Gaussian noise with zero mean and variance, σ^2.

The following subsection present the 3D GBSM channel models for CA and URA transmitters.

Proposed 3D GBSM Models

We consider the 3GPP's standard, based on the GBSM method [90,93,99], to provide a new 3D channel model in which the TX antenna is modeled as URA or CA. The main parameters of importance in the 3D channel model are; delay spread (DS), angle of arrival (AoA), azimuth of departure (AoD), elevation angle of arrival (EoA) and departure (EoD) [17,100,101]. In addition, the 3GPP standard under consideration presents the elevation angle of the antenna boresight into the channel and allows for dynamic adaption of the antenna's downtilt angles θ_{tilt}. This provides various advantages for 3D beamforming leading to significant improvement in system performance [95]. The 3D channel model is illustrated in Figure 4.

From Figure 4 and the 3GPP's model, the effective channel between the sth TX antenna port with M subpath and the uth receiver antenna port, as stated in [21,92], is

$$\left[\mathbf{H}_{s,u}^{\text{3D}}\right] = \sqrt{\frac{P_n \sigma_{SF}}{M}} \sum_{n=1}^{N} \kappa_n \left[\begin{array}{l} \sqrt{G_{TX}^{\text{3D}}(\phi_n^{AoD}, \theta_n^{AoD}, \theta_{tilt})} \sqrt{G_{RS}^{\text{3D}}(\varphi_n^{AoA}, \vartheta_n^{AoA})} \\ \times \left[a_{RX}(\varphi_n^{AoA}, \vartheta_n^{AoA})\right]_u \left[a_{TX}(\phi_n^{AoD}, \theta_n^{AoD})\right]_s \end{array} \right] \tag{3}$$

where κ_n is the complex random amplitude of the nth path and $s = 1, ..., N_{TX}$, $u = 1, ..., N_{RS}$, $(\phi_n^{AoD}, \theta_n^{AoD})$ are the azimuth and elevation angles-of-departure (AoD), respectively.

$(\varphi_n^{AoA}, \vartheta_n^{AoA})$ are the azimuth and elevation angles-of-arrival (AoA) of the nth path, respectively. The gain of antenna array at the TX is

$$G_{TX}^{\text{3D}}\left(\phi_n^{AoD}, \theta_n^{AoD}, \theta_{tilt}\right) \approx G_{TX,H}\left(\phi_n^{AoD} G_{TX,V}(\theta_n^{AoD}, \theta_{tilt})\right) \tag{4}$$

The responses of the antenna array are; $\left(a_{RX}\left(\varphi_n^{AoA}, \vartheta_n^{AoD}\right)\right)$ and $\left(a_{TX}\left(\phi_n^{AoD}, \theta_n^{AoD}\right)\right)$.

Following the approach in [90], the precise 3D antenna radiation pattern in both the horizontal ($G_{TX,H}$) and vertical ($G_{TX,V}$) planes is provided by [21],

$$G_{TX,H}(\phi^{AoD}) = -12\left(\frac{\phi^{AoD}}{\phi_{3dB}}\right)^2 \tag{5}$$

and

$$G_{TX,V}(\theta^{AoD}, \theta_{tilt}) = -12\left(\frac{\theta^{AoD} - \theta_{tilt}}{\theta_{3dB}}\right)^2 \tag{6}$$

where ϕ^{AoD} is the horizontal azimuth angle between the user and the array's boresight, θ^{AoD} is the vertical elevation angle between the user and the array's boresight, and ϕ_{3dB} and θ_{3dB} are the horizontal and vertical half-power beamwidths, respectively.
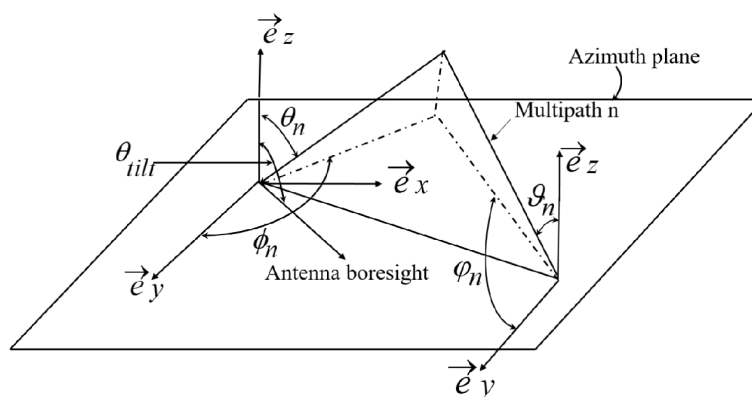
θ_{tilt} = Elevation angle of the boresight

θ_n, ϑ_n = Elevation AoD & AoA of the nth path respectively

ϕ_n, φ_n = Azimuth AoD & AoA of the nth path respectively

Figure 4. 3D channel model.

In this study, we consider URA or CA at the TX serving a single antenna RS with half-duplex connection in the model. The path between TX and RS has a single bounce cluster giving us N paths.

For the URA configuration indicated in Figure 5a, the location vector of the antenna element is as follows. As given in [102], the steering vector of the nth propagation path using the URA antenna topology shown in Figure 5a is

$$a_n(\theta_n^{AoD}, \phi_n^{AoD}) = Z\sin\left(\theta_n^{AoD}\sin(\bar{\beta} + \phi_n^{AoD})\right) \tag{7}$$

where $\bar{\beta} = \tan^{-1}(Z_z/Z_y)$, Z, Z_z and Z_y can be determined from Figure 5a. The figure shows the scalar z and y axes, where Z is defined [21] as,

$$Z = \sqrt{Z_z^2 + Z_y^2} \tag{8}$$

where,

$$\begin{aligned} Z_z &= 2\pi dz(n-m)/\lambda, \\ Z_y &= 2\pi dy(p-q)/\lambda \quad \text{and} \\ \varphi_s &= \cos^{-1}(Z_z/Z_y) \end{aligned} \tag{9}$$

are obtained. (m, p) and (n, q) are the coordinates of the elements shown in Figure 5a. The position of the URA antenna element at the TX can be determined by $Z \angle \bar{\beta}$. d_r is the distance between the receiving ports of the RX antennas. The location vector of sth transmit element of the URA is expressed as $v_t \cdot x_s = \cos(\phi - \varphi_s) \sin \theta$ where $\varphi_s = 2\pi(n-1)/N$. The array response of the sth of TX antenna port of URA considering (3) is given by

$$[a_{TX}(\phi_n^{AoD}, \theta_n^{AoD})]_s = \exp\left(ikZ \cos(\phi_n^{AoD} - \varphi_s) \sin \theta_n^{AoD}\right) \tag{10}$$

Similarly, the response of uth UE antenna port with regard to the 3D channel model is

$$[a_{RX}(\varphi_n^{AoA}, \vartheta_n^{AoA})]_u = \exp\left(ik(u-1)d_r \sin \varphi_n^{AoA} \sin \vartheta_n^{AoA}\right) \tag{11}$$

Thus, the 3D GBSM channel model of the URA transmitter configuration of the proposed mMIMO CR-NOMA model in Figure 3 is

$$H_{s,u}^{\text{URA}} = \sqrt{\frac{P_n \sigma_{SF}}{M}} \sum_{n=1}^{N} \kappa_n \left[\begin{array}{c} \sqrt{G_{TX}^{3D}(\phi_n^{AoD}, \theta_n^{AoD}, \theta_{tilt})} \exp\left(ikZ \cos(\phi_n^{AoD} - \varphi_s) \sin \theta_n^{AoD}\right) \\ \times \sqrt{G_{RS}^{3D}(\varphi_n^{AoA}, \vartheta_n^{AoA})} \exp\left(ik(u-1)d_r \sin \varphi_n^{AoA} \sin \vartheta_n^{AoA}\right) \end{array} \right] \tag{12}$$

where P_n denotes power of the nth path, σ_{SF} is lognormal shadow fading of the nth path. N is the number of propagation path, M is the number of subpath per path, d_r is the separation between the receiving antenna ports, k is the wave number and G_{RS}^{3D} is the gain of the RS antenna.
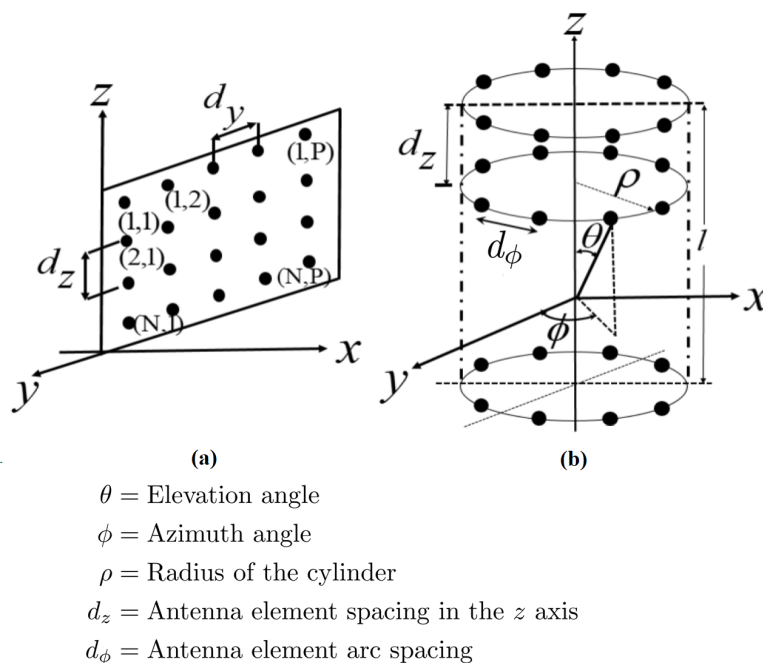

θ = Elevation angle
ϕ = Azimuth angle
ρ = Radius of the cylinder
d_z = Antenna element spacing in the z axis
d_ϕ = Antenna element arc spacing

Figure 5. Geometric structure of (**a**) rectangular array (URA) and (**b**) cylindrical array (CA).

In the case of CA, Figure 5b, considering the array dimension of CA as $l = 4\lambda$ with radius given by $\rho = 4\lambda/l$, if $d_z = 4\lambda/M$ is the wavelength distance in meters between antenna elements on the first and second position in the z direction. Then $4\lambda(m-1)/M$ wavelengths may be used to estimate the placement of the third and following antenna components, where $m = 1, ..., M$ is the number of antenna elements on a ring in the z-axis, and λ is the wavelength in meters. The angular position of the nth element of the mth of CA on the x-y plane is expressed as $\varphi_s = 2\pi(n-1)/N$. Consequently, the location vector of

the elements is $v_t \cdot x_s = \cos(\phi - \varphi_s) \sin \theta$. Furthermore, the array response of sth transmit antenna port of the CA is given by

$$\left[a_{TX}(\phi_n^{AoD}, \theta_n^{AoD}) \right]_s = \exp\left(ik\rho \frac{4\lambda(m-1)}{M} \cos(\phi_n^{AoD} - \varphi_s) \sin \theta_n^{AoD} \right) \tag{13}$$

Similarly, the response of the uth UE antenna port using the 3D channel model is

$$\left[a_{RX}(\varphi_n^{AoA}, \vartheta_n^{AoA}) \right]_u = \exp\left(ik(u-1)d_r \sin \varphi_n^{AoA} \sin \vartheta_n^{AoA} \right) \tag{14}$$

The final 3D GBSM channel model of the proposed model in Figure 3 between a single antenna receiving port u^{th} and a CA transmitter's transmit antenna port s^{th} is given by [21]

$$H_{s,u}^{\text{CA}} = \sqrt{\frac{P_n \sigma_{SF}}{M}} \sum_{n=1}^{N} \kappa_n \left[\begin{array}{l} \sqrt{G_{TX}^{3D}(\phi_n^{AoD}, \theta_n^{AoD}, \theta_{tilt})} \\ \times \exp\left(ik\rho(4\lambda(m-1)/M) \cos(\phi_n^{AoD} - \varphi_s) \sin \theta_n^{AoD} \right) \\ \times \sqrt{G_{RS}^{3D}(\varphi_n^{AoA}, \vartheta_n^{AoA})} \exp\left(ik(u-1)d_r \sin \varphi_n^{AoA} \sin \vartheta_n^{AoA} \right) \end{array} \right] \tag{15}$$

3. Achievable Rates, Outage Probabilities and Bit-Error-Rates Analysis

3.1. Transmission between TX and RS

Here, we consider a two-hop downlink communication between a TX and two UEs through a dedicated RS and apply the 3D GBSM channel to the TX$-$RS and RS$-$UEs communication links.

We analyze the transmission between TX and RS in the proposed 3D GBSM mMIMO CR-NOMA system model [103–105] with large antenna transmitters such as URA or CA in Figure 5, and as illustrated in Figure 3. Two key assumptions are taken into account in the system model. Firstly, there is no direct communication link between TX and UEs. Secondly, users are close to each other in a half-duplex communication mode and have a single antenna each for reception. The communication between TX and UEs takes two stages. During the first stage, the TX transmit a superposition of two distinct signals ($\mathbf{x}$) to the relay, from which the relay re-transmits to all UEs. The received signal (y_{RS}) at the relay can be expressed as

$$y_{RS} = \sqrt{\alpha_R} \mathbf{h}_{TX} \mathbf{x} + \eta_R \tag{16}$$

where $\mathbf{h}_{TX}$ is the proposed 3D GBSM [103–106] channel coefficient between the TX and RS, η_R is the additive white Gaussian noise (AWGN) with unit variance. $\alpha_R = d_{SR}^{-\delta}$ is the distance-dependent path loss, where d_{SR} is the distance between TX and RS, and δ is the path loss exponent. Again, using the concept of NOMA, users are arranged in ascending order according to the power allocation factors such that $\alpha_1 < \alpha_2$, where the superimposed signal ($\mathbf{x}$) is given in (1).

3.2. Transmission between RS and UE

3.2.1. Application of AF Coding Scheme

The relay amplifies the incoming signal in the second stage using an AF coding scheme and an amplification factor of (18). Thus, the received signal (y_k^{AF}) at the kth user (UE$_k$) is

$$\begin{aligned} y_k^{\text{AF}} &= y_{RS} \mathbf{h}_{R,k} \sqrt{\beta_k} G + n_k \\ &= \mathbf{h}_{R,k} \sqrt{\beta_k} G \sqrt{\alpha_R} \mathbf{h}_{TX} \mathbf{x} + \mathbf{h}_{R,k} G \sqrt{\beta_i} \eta_R + \eta_k \end{aligned} \tag{17}$$

where n_k is the complex additive Gaussian noise at k^{th} user with $\mathbb{CN}(0, \sigma^2)$, $\mathbf{h}_{R,k}$ is a 3D channel model following (3) and the β_k is path loss between the RS and k^{th} UE. G is the amplifying factor [107] given by

$$G = \sqrt{\frac{\alpha_g^2}{P_s|\mathbf{h}_{TX}^2| + \sigma_R^2}} \tag{18}$$

where $\alpha_g^2 = \varrho(1-d)^{-k}$ is a non-fading variable path gain, $\varrho = 1$ is the reference distance's path-loss exponent, d_0 is the reference distance, $d = d_e/d_0$ is the normalized relay distance from the source, and k is the path-loss exponent of the TX−RS channel. The effective distance d_e is the actual distance of TX−RS in meters, where the cell radius is d_0. To reduce the impact of inter-user interference on each user, SIC at the destination's receiver [108]. The effective users' channel gains determine SIC decoding order in ascending order, that is $|\mathbf{h}_{R,1}|^2 \geq |\mathbf{h}_{R,2}|^2$. The signal-to-interference noise ratio ($\gamma_{1,2}^{\text{AF}}$) for the strong user (UE$_1$) to decode x_2 by applying SIC processing is given in [109] as

$$\gamma_{1,2}^{\text{AF}} = \frac{\alpha_2 \gamma^2 |\mathbf{h}_{TX}|^2 |\mathbf{h}_{R,2}|^2}{\gamma^2 |\mathbf{h}_{TX}|^2 |\mathbf{h}_{R,1}|^2 \alpha_1 + \gamma\left(|\mathbf{h}_{TX}|^2 + |\mathbf{h}_{R,1}|^2\right) + 1} \tag{19}$$

After decoding the message of UE$_2$ and subtracting it, UE$_1$ decodes its signal with the following SINR ($\gamma_{R,1}^{\text{AF}}$) between the RS and UE$_1$ [109].

$$\gamma_{R,1}^{\text{AF}} = \frac{\alpha_1 \gamma^2 |\mathbf{h}_{TX}|^2 |\mathbf{h}_{R,1}|^2}{\gamma\left(|\mathbf{h}_{TX}|^2 + |\mathbf{h}_{R,1}|^2\right) + 1} \tag{20}$$

The SINR ($\gamma_{R,2}^{\text{AF}}$) between the RS and the UE$_2$ to detect its own message is expressed in [109] as

$$\gamma_{R,2}^{\text{AF}} = \frac{\alpha_2 \gamma^2 |\mathbf{h}_{TX}|^2 |\mathbf{h}_{R,2}|^2}{\gamma^2 |\mathbf{h}_{TX}|^2 |\mathbf{h}_{R,2}|^2 \alpha_1 + \gamma\left(|\mathbf{h}_{TX}|^2 + |\mathbf{h}_{R,2}|^2\right) + 1} \tag{21}$$

where γ gives the average signal-to-noise ratio (SNR).

3.2.2. Application of DF Coding Scheme

During the first time slot, the TX transmits a superimposed signal according to NOMA principles to the relay. The achievable rates ($R_{x_1}^{\text{RS}}$ and $R_{x_2}^{\text{RS}}$) for the relay to decode x_1 and x_2 are given [109] by

$$R_{x_1}^{\text{RS}} = B\log_2\left(1 + \frac{\alpha_1 \gamma |\mathbf{h}_{TX}|^2}{\alpha_2 \gamma |\mathbf{h}_{TX}|^2 + 1}\right) \tag{22}$$

and

$$R_{x_2}^{\text{RS}} = B\log_2\left(1 + \alpha_2 \gamma |\mathbf{h}_{TX}|^2\right) \tag{23}$$

where α_1 and α_2 are power allocation factors associated with x_1 and x_2, respectively. UE$_1$'s signal x_1 and UE$_2$'s signal x_2 are the vector elements of $\mathbf{x}$.
Given that the relay can decode the signal from TX of the two NOMA users, the observable signal (y_k^{DF}) at UE$_1$ and UE$_2$ in the second slot may be stated as

$$y_k^{\text{DF}} = \mathbf{h}_{R,k}\sqrt{\beta_k}\mathbf{x} + \eta_k \tag{24}$$

where $k = $ UE, $\beta_k > 0$ denotes the power allocation factor of the kth UE. Here, $\beta_1 + \beta_2 = 1$. Following the principle of NOMA scheme, the decoding order at the relay is $x_1 \rightarrow x_2$. The

relay first detects x_1 by treating x_2 as noise. It then subtracts x_1 from the y_{RS} in (16) to identify x_2. By employing SIC, the SINR ($\gamma_{1,2}^{\text{DF}}$) at UE$_1$ to detect x_2 is given [109] by

$$\gamma_{1,2}^{\text{DF}} = \frac{\beta_2 \gamma |\mathbf{h}_{R,1}|^2}{\beta_1 \gamma |\mathbf{h}_{R,1}|^2 + 1} \tag{25}$$

The SINR ($\gamma_{R,1}^{\text{DF}}$) for UE$_1$ to detect its own signal is

$$\gamma_{R,1}^{\text{DF}} = \beta_1 \gamma |\mathbf{h}_{R,1}|^2 \tag{26}$$

Similarly, the SINR ($\gamma_{R,2}^{\text{DF}}$) at UE$_2$ is given [109] by

$$\gamma_{R,2}^{\text{DF}} = \frac{\beta_2 \gamma |\mathbf{h}_{R,2}|^2}{\beta_1 \gamma |\mathbf{h}_{R,2}|^2 + 1} \tag{27}$$

3.3. Achievable Rates Analysis

The maximum rate in the channel where the BER tends to zero [110] describes the achievable rate of the system. When the CSI is unknown at the transmitter, if separate equi-powered transmissions are assumed, the achievable rates of the UEs can be determined using SINR values. From (19)–(21), the achievable rates of the UEs using AF coding scheme are respectively given by

$$R_{UE_1}^{\text{AF}} = B log_2(1 + \gamma_{R,1}^{\text{AF}}) \ \text{ and } \ R_{UE_2}^{\text{AF}} = B log_2(1 + \gamma_{R,2}^{\text{AF}}) \tag{28}$$

For DF coding scheme, the achievable rates at the destination nodes from (25)–(27) are

$$\begin{aligned} R_{UE_1}^{\text{DF}} &= \min[R_{x_1}^{\text{RS}}, B log_2(1 + \gamma_{R,1}^{\text{DF}})] \quad \text{and} \\ R_{UE_2}^{\text{DF}} &= \min[R_{x_2}^{\text{RS}}, B log_2(1 + \gamma_{R,2}^{\text{DF}})] \end{aligned} \tag{29}$$

The relay transmits the decoded signals to all UES in the second time slot.

3.4. Outage Probabilities Analysis

To determine the likelihood that a data stream may have an outage event where the achievable rate is lower than the encoded data rate [15], we examine the outage probability where the UE$_1$ can detect x_2 and x_1. Given the previous definition, the outage probability (P_1) of UE$_1$ with the threshold SNRs of CR-NOMA users UE$_1$ and UE$_2$ (denoting Ω_1, Ω_2, respectively) may be described in [109] as

$$P_1 = \left[1 - P_r(\xi_{\text{RS}} \geq \xi'_{\Omega_2}, \xi_{\text{RS}} \geq \xi'_{\Omega_1}) \right] \times \left[1 - P_r(\xi_{l,2}^X \geq \xi'_{\Omega_2}, \xi_1^X \geq \xi'_{\Omega_1}) \right] \tag{30}$$

where $\xi'_{\Omega_1} = 2^{2\tilde{\mathcal{R}}_1} - 1$ and $\xi'_{\Omega_2} = 2^{2\tilde{\mathcal{R}}_2} - 1$ are the decoding threshold with $\tilde{\mathcal{R}}_1$ and $\tilde{\mathcal{R}}_2$ being the target rate of UE$_1$ and UE$_2$, respectively. ξ_{RS} is the SINR between TX and RS, $\tilde{\xi}_{\text{RS}}$ is the decoding threshold of the direct transmission to the RS. ξ_1^X and ξ_2^X are the SINR defined at (20), (21), (26) and (27), where X in the equation denotes AF or DF coding scheme. Similarly, the outage probability (P_2) of UE$_2$ is

$$P_2 = P_r(\xi_{\text{RS}} < \xi'_{\Omega_2}, \ \xi_2^X < \xi'_{\Omega_2}) \tag{31}$$

3.5. Bit-Error-Rates (BER) Analysis

We give the Bit-error analysis for the proposed CR-NOMA system in accordance with the guidelines in [111,112]. The average error probability ($P_e^{\text{UE}_1}$) of the UE$_1$ when its symbols are identified properly and erroneously via SIC processing is shown in [111] as

$$P_e^{\mathrm{UE}_1} = \frac{1}{2}\left(1 - \sqrt{\frac{\gamma_{\mathcal{B}_1}}{2 + \gamma_{\mathcal{B}_1}}}\right) + \frac{1}{8}\left[\sqrt{\frac{\gamma_{\mathcal{B}_2}}{2 + \gamma_{\mathcal{B}_2}}} - \sqrt{\frac{\gamma_{\mathcal{B}_3}}{2 + \gamma_{\mathcal{B}_3}}} + \sqrt{\frac{\gamma_{\mathcal{B}_4}}{2 + \gamma_{\mathcal{B}_4}}} - \sqrt{\frac{\gamma_{\mathcal{B}_5}}{2 + \gamma_{\mathcal{B}_5}}}\right] \tag{32}$$

where ε_1 and ε_2 are the UE_1 and UE^2 signal energies, respectively. The SNRs of different constellation points of x_1 and x_2 are given by

$$
\begin{aligned}
\gamma_{\mathcal{B}_1} &= \frac{\varepsilon_1}{N_0}\mathbb{E}\left[|\mathbf{h}_{R,1}|^2\right] \\
\gamma_{\mathcal{B}_2} &= \frac{\left(\sqrt{2\varepsilon_2} + \sqrt{\varepsilon_1}\,\right)^2}{N_0}\mathbb{E}\left[|\mathbf{h}_{R,1}|^2\right] \\
\gamma_{\mathcal{B}_3} &= \frac{\left(\sqrt{2\varepsilon_2} - \sqrt{\varepsilon_1}\,\right)^2}{N_0}\mathbb{E}\left[|\mathbf{h}_{R,1}|^2\right]
\end{aligned}
\tag{33}
$$

and

$$
\begin{aligned}
\gamma_{\mathcal{B}_4} &= \frac{\left(2\sqrt{2\varepsilon_2} + \sqrt{\varepsilon_1}\,\right)^2}{N_0}\mathbb{E}\left[|\mathbf{h}_{R,1}|^2\right] \\
\gamma_{\mathcal{B}_5} &= \frac{\left(2\sqrt{2\varepsilon_2} - \sqrt{\varepsilon_1}\,\right)^2}{N_0}\mathbb{E}\left[|\mathbf{h}_{R,1}|^2\right]
\end{aligned}
\tag{34}
$$

Equation (33) represents the condition that UE_1 is able to detect its signals correctly, whereas (34) represents the condition that the signals are incorrectly detected.

Similarly, the total average BER ($P_e^{\mathrm{UE}_2}$) performance of UE_2 from [111] is

$$P_e^{\mathrm{UE}_2} = \frac{1}{4}\left[\left(1 - \sqrt{\frac{\gamma_{\mathcal{A}_1}}{2 + \gamma_{\mathcal{A}_1}}}\right) + \left(1 - \sqrt{\frac{\gamma_{\mathcal{A}_2}}{2 + \gamma_{\mathcal{A}_2}}}\right)\right] \tag{35}$$

where $\gamma_{\mathcal{A}_1}$ and $\gamma_{\mathcal{A}_2}$ are the SNRs of different signal constellation points expressed as

$$
\begin{aligned}
\gamma_{\mathcal{A}_1} &= \frac{\left(\sqrt{2\varepsilon_2} + \sqrt{\varepsilon_1}\,\right)^2}{N_0}\mathbb{E}\left[|\mathbf{h}_{R,2}|^2\right] \\
\gamma_{\mathcal{A}_2} &= \frac{\left(\sqrt{2\varepsilon_2} - \sqrt{\varepsilon_1}\,\right)^2}{N_0}\mathbb{E}\left[|\mathbf{h}_{R,2}|^2\right]
\end{aligned}
\tag{36}
$$

4. Numerical Results and Analyses

In this section, we validate the proposed 3D channel model for an mMIMO CR-NOMA system through simulation using the MatLab numeric computing platform for evaluation purposes. We compared the results to a system using CBSM channel model such as Rayleigh fading channel [17,19]. The major application of CBSM is for assessing theoretical performance because it is imprecise at simulating channel characteristics for real large MIMO systems.

We evaluate the proposed 3D GBSM models by setting the AoA cluster (ϕ, θ) to 0.7, and AoA offset standard deviations, $(\sigma_{\Delta\phi}, \sigma_{\Delta\theta})$ to -0.3 at 2.6 GHz carrier frequency [113]. The proposed system model uses 5G network operating bandwidth of 200 MHz [114]. We consider the entire physical space of URA antenna components at the TX as $l = 4\lambda$ on both the y and z axes.

Similarly, for the CA, adjacent antenna element are spaced by $l = 4\lambda$ on the z axis and are located at a maximum radius of $\rho = 2\pi/l$ from the cylinder center to x, y plane. The CA has a $2 \times N_t$ number of components, and in the azimuth domain, there are two circular arrays with $N_t = 4$ elements each. We studied a $N_t \times N_t$ array element in the case of the URA, where N_t is the number of antenna elements in a row or column.

For each TX antenna topology, we calculated the channel coefficient as the distance between the sth transmit antenna port and the uth receive antenna port. In order to validate

the proposed model, we considered $\theta_{tilt} = 95°$, $\theta_{3dB} = 15°$ and $\phi_{3dB} = 70°$ at the TX for the 3D channel modeling between the TX, RS and UEs in Figure 3. Table 2 gives the summary of simulation parameters.

Additionally, the power of azimuth spectrum (PAS) arriving at the RS, multipath components for each AoA, and the multipath delay associated with AoD are all represented as Laplacian distributions with specified 3GPP specifications. For the cooperative communication at the relay, we considered DF and AF with the proposed 3D GBSM between the TX, RS and UEs. The OP, achievable rate and BER are determined for each relaying scheme and compared with the results of a system using CBSM, as illustrated in Figure 2.

Table 2. Simulation Parameters.

Parameter	Value
Frequency	2.6 GHz
Operating bandwidth	200 MHz
θ_{tilt}	95°
θ_{3dB}	15°
ϕ_{3dB}	70°
Antenna configuration	URA, CA
Number of clusters	1
Number of users	2
Channel model	3D GBSM
Path-loss exponent	4
Environment	Urban Macrocell
UE power allocations	$\alpha_1 = 0.2, \alpha_2 = 0.8$

4.1. Achievable Rate Performance

For achievable rate analysis, (28) and (29) were used to determine the achievable rates of AF and DF. In Figure 6, the UE_1 achievable rate obtained using DF coding scheme is higher than that of the AF coding scheme across the entire SNR, irrespective of the TX type used in the proposed 3D GBSM channel model. It can also be seen from the comparison of the results of DF and AF for CA channel model that the capacities of UE_1 and UE_2 have similarities with higher capacity values of AF coding scheme at higher SNR values.

4.2. BER Performance

For BER performance evaluation, we use (12) and (15) that are based on the channel coefficients between the TX, RS and UEs. The transmissions between TX and UEs through were further examined using (20) and (21). The BER of UE_1 and UE_2 was estimated using (32) and (35), respectively. Figures 7 and 8 show the BER for various SNR values in dB for AF and DF coding schemes. The number of TX antenna elements in the proposed 3D GBSM channel model is sixty-eight (68) for both URA and CA. The performance of the 3D model using CA at the transmitter achieves better at low SNR values as compared with the URA in Figures 7 and 8. In both cases of Figures 7 and 8, the performance of UE_1 is better than UE_2. This is because the received power at UE_1 is higher than that of UE_2 since it is closer to the RS.
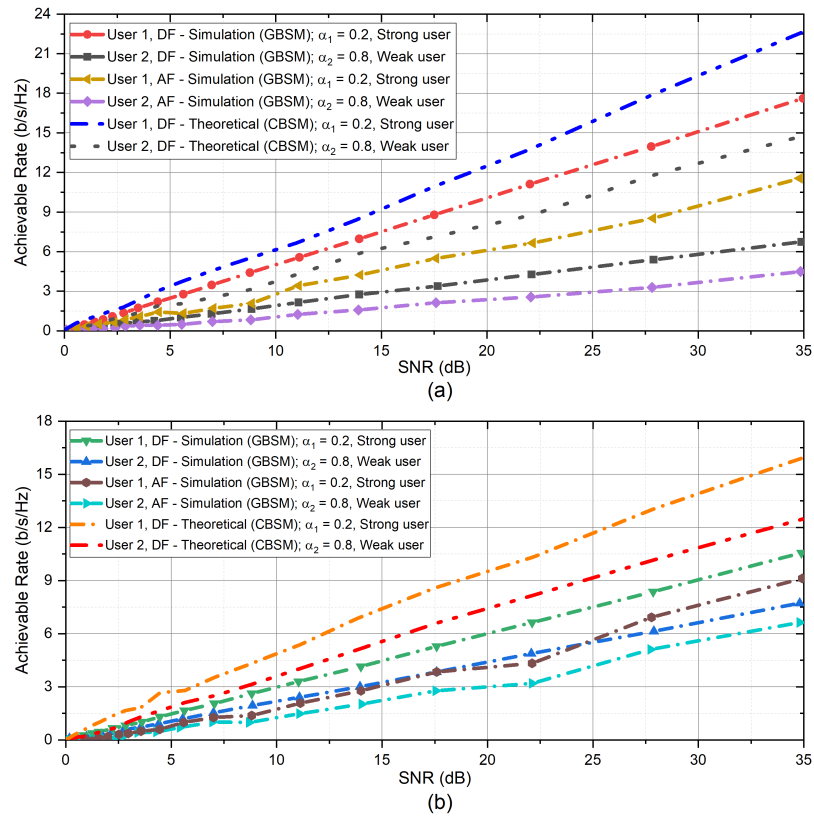
Figure 6. Achievable rates of DF and AF schemes of the proposed 3D channel model with (**a**) URA and (**b**) CA.
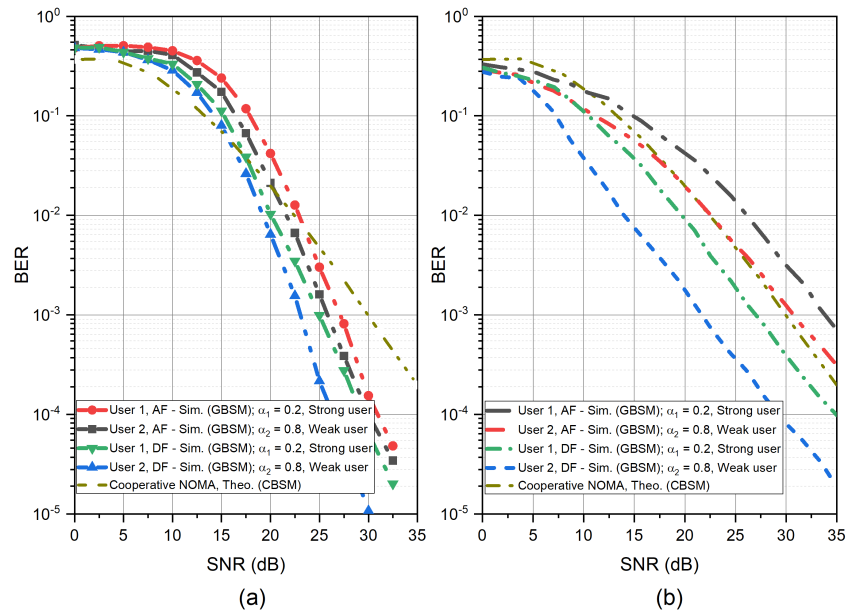

Figure 7. BER of AF and DF schemes of the proposed 3D channel model with (**a**) 3D URA and (**b**) 3D CA.
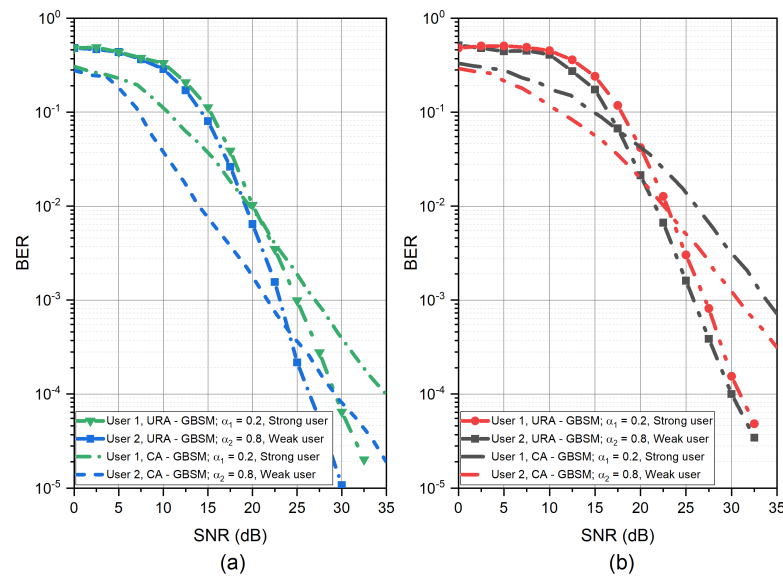
Figure 8. BER comparison of AF and DF schemes with (**a**) DF and (**b**) AF coding schemes.

The Table 3 lists the BER performance of the CR-NOMA system with the proposed GBSM channel with URA antenna array configuration at the TX using AF or DF coding schemes at the RS. The BER of the DF coding scheme at 20 dB shows performance similar to prior work that uses the theoretical channel model (CBSM channel model). On the other hand, the AF coding scheme's BER performance of the proposed model performed worse than CBSM with AF coding scheme.

Table 3. Comparison of average BER with prior works.

Ref.	Relay Schemes	Channel Model & Antenna Type	No. of Users	SNR (dB)	BER
Proposed model	AF	GBSM, multiple antenna TX, single antenna RS and UE	2	5	$10^{-2.50}$
				20	$10^{-2.85}$
	DF			5	$10^{-2.05}$
				20	$10^{-2.40}$
[15]	CpF	CBSM, single antenna TX, RS and UE	2	5	$10^{-3.80}$
				20	$10^{-5.00}$
	AF			5	$10^{-2.80}$
				20	$10^{-3.00}$
	DF			5	$10^{-1.80}$
				20	$10^{-2.10}$
[43]	AF	CBSM, single antenna TX, RS and UE	1	5	$10^{-1.50}$
				20	$10^{-2.70}$
	DF			5	$10^{-1.00}$
				20	$10^{-2.70}$
[115]	AF	CBSM, single antenna TX, RS and UE	2	5	$10^{-2.00}$
				20	$10^{-2.70}$
[116]	DF	CBSM, multiple antenna TX, RS and UE	2	5	$10^{-1.95}$
				20	$10^{-4.96}$

The reason is due to the high unpredictability of the GBSM parameters and high computational complexity, which causes a significant amount of noise signal in the channel and at the RS.

4.3. Outage Probability (OP) Performance

The analysis cannot be complete without examining the outage probability. Employing 3D GBSM URA and CA channel models in (12) and (15), we demonstrate the outage

probability of mMIMO CR-NOMA as a function of transmitting SNR in Figure 9. The performance disparity between the two users, UE_1 and UE_2, spreads across the whole range of SNR. This is demonstrated in the OP outcome of the 3D URA system. It is important to note that modifying the transmitter array arrangement and expanding the TX's antenna elements while keeping a single antenna at the relay node can dramatically increase system outage performance.

Furthermore, it demonstrates that UE_2's outage performance is poorer than UE_1. This means that using less transmit power at the relays lowers the hop's outage performance, which in turn affects the total outage performance. This is because signal x_1, which is regarded as noise, causes interference in the communication link between the RS and UE_2. UE_1 signal x_1 is amplified when the UE_2's signal (x_2) is amplified by RS with AF coding scheme. The interference impacts the decoding performance of the RS when using the AF coding scheme for the connection between RS$-UE_2$. Again, Figure 9 shows outage probabilities of two users with AF and DF relay coding schemes. It can be seen that under the 3D URA channel model, the OP of the DF coding scheme achieves higher performances than the AF coding scheme.

We further perform analysis using the CA channel model. Here, the OP of UE_1 using AF coding scheme performs better than that of the DF coding scheme, unlike that of the OP of the URA channel model. Generally, the performance of the system using the CA is better than URA for both AF and DF coding schemes. In Table 4, we compare OP performance at SNR of 15 dB of the proposed 3D GBSM channel models with prior works that use CBSM models.
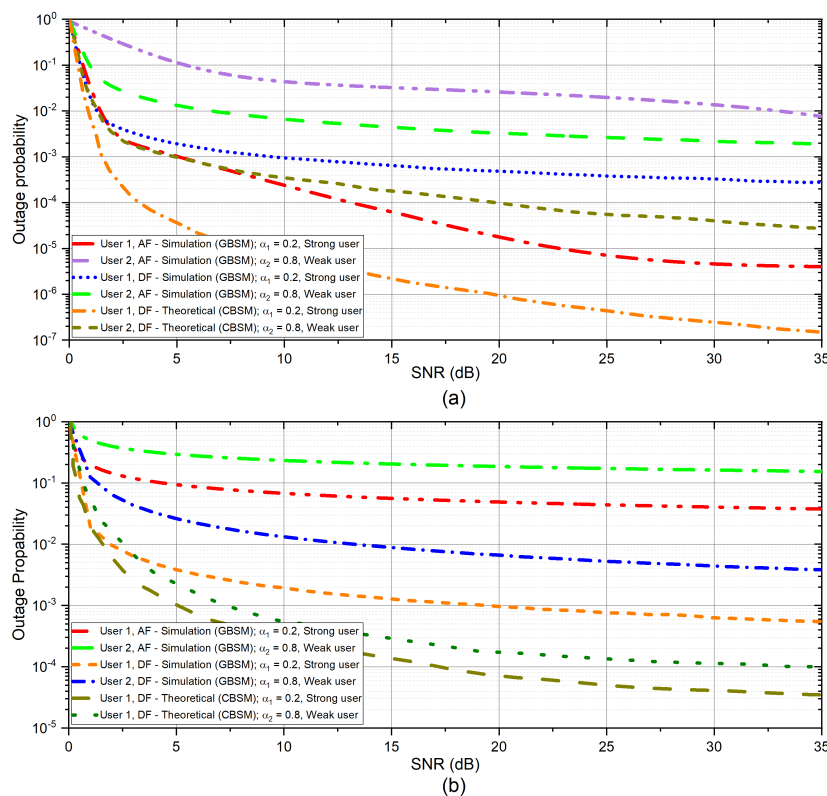

Figure 9. Outage probability comparison of two users using AF and DF schemes of the proposed channel models with (**a**) CA and (**b**) URA.

Table 4. Comparison of Outage Probability with prior works at SNR of 15 dB.

Ref.	Relay Schemes	Channel Model & Antenna Type	No. of Users	No. of Relays	OP
Proposed model	AF DF	GBSM, multiple antenna TX, single RS and UE	2	1	$10^{-1.25}$ $10^{-2.50}$
[15]	CpF AF DF	CBSM, single antenna TX, RS and UE	2	1	$10^{-3.40}$ $10^{-2.00}$ $10^{-1.50}$
[78]	AF	CBSM, multiple antenna TX and RS, single antenna UE	M	1	$10^{-5.38}$
[117]	AF DF	CBSM, single antenna TX, RS and UE	2	M	$10^{-1.00}$ $10^{-0.80}$
[118]	DF	CBSM, multiple antenna TX, single antenna RS and UE	3	1	$10^{-2.45}$
[119]	DF	CBSM, multiple antenna TX and UE, single antenna RS	2	1	$10^{-0.28}$

5. Conclusions and Future Scope

In this paper, different from previous works on mMIMO CR-NOMA system, we have presented a 3D GBSM channel model between TX−RS and RS−UEs communication links. We examined a two-stage downlink mMIMO CR-NOMA system with the 3D GBSM channel model where the transmitter is represented by CA or URA. We have undertaken performance analyses of the proposed system model with simulations and compared it with the theoretical results of systems using CBSM. Generation of 3D GBSM channel model is complex, therefore, to minimize the computational complexity of the channel, we defined the antenna location vector based on the physical dimension of the antenna configuration. The proposed 3D GBSM channel model incorporates various network coding schemes such as DF and AF for better channel and system performance. For performance analysis, we derived the probability of an outage, the achievable rate and the bit-error rate for the two-stage system. According to the results, the combination of CA and AF gives a better outage probability. Finally, even though the proposed 3D GBSM channel model has a higher computational cost in terms of complexity, the results reveal that the performance difference between the theoretical channel model (CBSM) and GBSM is minimal. The work can further be extended to cover millimeter-wave CR-NOMA with multiple antenna at the TX, RS and UEs. Again, the effect of spatial correlation of antenna array configuration on the performance of 3D GBSM in CR-NOMA systems presents good future research opportunities.

Abbreviations

The following abbreviations are used in this manuscript:

NOMA	Non-Orthogonal Multiple Access
5G	Fifth Generation
SIC	Successive Interference Cancellation
CR-NOMA	Cooperative Relay Non-Orthogonal Multiple Access
mMIMO	Massive Multiple-Input Multiple-Output
CBSM	Correlated-Based Stochastic Channel Model
GBSM	Geometric-Based Stochastic Channel Model
3GPP	Third Generation Partnership Project
3D	Three Dimension
URA	Uniform Rectangular Array
CA	Cylindrical Array
OP	Outage Probability
AF	Amplify-and-Forward
DF	Decode-and-Forward
OMA	Orthogonal Multiple Access
MIMO	Multiple-Input Multiple-Output
CSI	Channel State Information
CF	Compress-and-Forward
CpF	Compute-and-Forward
BER	Bit-Error-Rate
EH	Energy Harvesting
BS	Base Station
SNR	Signal-to-Noise Ratio
TX	Transmitter
UE	User Equipment
RS	Relay Station
P_s	Total Transmit Power
DL	Downlink
DS	Delay Spread
AoA	Angle of Arrival
AoD	Azimuth of Departure
EoD	Elevation Angle of Departure
EoA	Elevation Angle of Arrival
AWGN	Additive White Gaussian Noise
d_{SR}	Distance between TX and Rs
SINR	Signal-to-Interference Noise Ratio
PAS	Power of Azimuth Spectrum

References

1. Penttinen, J.T. *5G Explained: Security and Deployment of Advanced Mobile Communications*; John Wiley & Sons: Hoboken, NJ, USA, 2019.
2. Shahraki, A.; Abbasi, M.; Piran, M.; Chen, M.; Cui, S. A comprehensive survey on 6g networks: Applications, core services, enabling technologies, and future challenges. *arXiv* **2021**, arXiv:2101.12475.
3. Osseiran, A.; Parkvall, S.; Persson, P.; Zaido, A.; Magnusson, S.; Balachandran, K. *5G Wireless Access Network*; Whitepaper; Ericsson: 2020.
4. Carugi, M. Key features and requirements of 5G/IMT-2020 networks. In Proceedings of the ITU Arab Forum on Emerging Technologies, Algiers, Algeria, 14–15 February 2018.
5. Yuan, M.; Song, D.; Li, B. A Comparative Study on Key Technologies of Ultra-Reliable Low Latency Communication. In Proceedings of the International Conference on Machine Learning for Cyber Security, Guangzhou, China, 8–10 October 2020; Springer: Berlin/Heidelberg, Germany, 2020; pp. 112–124.

6. Carcel, J.L.; Mouhouche, B.; Fuentes, M.; Garro, E.; Gomez-Barquero, D. IMT-2020 key performance indicators: Evaluation and extension towards 5G new radio point-to-multipoint. In Proceedings of the 2019 IEEE International Symposium on Broadband Multimedia Systems and Broadcasting (BMSB), Jeju, Korea, 5–7 June 2019; pp. 1–5.

7. Akbar, A.; Jangsher, S.; Bhatti, F.A. NOMA and 5G emerging technologies: A survey on issues and solution techniques. *Comput. Netw.* **2021**, *190*, 107950.

8. Basnayake, V.; Jayakody, D.N.K.; Sharma, V.; Sharma, N.; Muthuchidambaranathan, P.; Mabed, H. A New Green Prospective of Non-orthogonal Multiple Access (NOMA) for 5G. *Information* **2020**, *11*, 89. https://doi.org/10.3390/info11020089.

9. Ghanami, F.; Hodtani, G.A.; Vucetic, B.; Shirvanimoghaddam, M. Performance analysis and optimization of NOMA with HARQ for short packet communications in massive IoT. *IEEE Internet Things J.* **2020**, *8*, 4736–4748.

10. Budhiraja, I.; Kumar, N.; Tyagi, S.; Tanwar, S.; Han, Z.; Suh, D.Y.; Piran, M.J. A Systematic Review on NOMA Variants for 5G and Beyond. *IEEE Access* **2021**, *9*, 85573–85644.

11. Islam, S.R.; Zeng, M.; Dobre, O.A.; Kwak, K.S. Nonorthogonal multiple access (NOMA): How it meets 5G and beyond. *arXiv* **2019**, arXiv:1907.10001.

12. Proakis, J.G.; Salehi, M.; Zhou, N.; Li, X. *Communication Systems Engineering*; Prentice Hall New Jersey:Upper Saddle River, NJ, USA 1994; Volume 2, Chapter 1, pp. 20–21.

13. Reddy, B.S.K.; Mannem, K.; Jamal, K. Software Defined Radio Based Non-orthogonal Multiple Access (NOMA) Systems. *Wirel. Pers. Commun.* **2021**, *119*, 1251–1273.

14. Islam, S.; Zeng, M.; Dobre, O.A. NOMA in 5G systems: Exciting possibilities for enhancing spectral efficiency. *arXiv* **2017**, arXiv:1706.08215.

15. Ntiamoah-Sarpong, K.; Huang, Z.; Wen, G.; Ampoma, A.E. Performance of non-orthogonal multiple access: Analysis using compute-and-forward cooperative relaying in 5G networks. *IET Commun.* **2020**, *14*, 3058–3064.

16. Laneman, J.N.; Tse, D.N.; Wornell, G.W. Cooperative diversity in wireless networks: Efficient protocols and outage behavior. *IEEE Trans. Inf. Theory* **2004**, *50*, 3062–3080.

17. Zheng, K.; Ou, S.; Yin, X. Massive MIMO channel models: A survey. *Int. J. Antennas Propag.* **2014**, *2014*, 848071.

18. Liu, Y.; Wang, C.X.; Lopez, C.F.; Goussetis, G.; Yang, Y.; Karagiannidis, G.K. 3D non-stationary wideband tunnel channel models for 5G high-speed train wireless communications. *IEEE Trans. Intell. Transp. Syst.* **2019**, *21*, 259–272.

19. Zhang, P.; Chen, J.; Yang, X.; Ma, N.; Zhang, Z. Recent research on massive MIMO propagation channels: A survey. *IEEE Commun. Mag.* **2018**, *56*, 22–29.

20. Zheng, K.; Zhao, L.; Mei, J.; Shao, B.; Xiang, W.; Hanzo, L. Survey of large-scale MIMO systems. *IEEE Commun. Surv. Tutor.* **2015**, *17*, 1738–1760.

21. Ampoma, A.E.; Wen, G.; Huang, Y.; Gyasi, K.O.; Tebe, P.I.; Ntiamoah-Sarpong, K. Spatial correlation models of large-scale antenna topologies using maximum power of offset distribution and its application. *IEEE Access* **2018**, *6*, 36295–36304.

22. He, D.; Ai, B.; Guan, K.; Wang, L.; Zhong, Z.; Kürner, T. The design and applications of high-performance ray-tracing simulation platform for 5G and beyond wireless communications: A tutorial. *IEEE Commun. Surv. Tutor.* **2018**, *21*, 10–27.

23. Zaghdoud, N.; Alouane, W.H.; Boujemaa, H.; Touati, F. Secure performance of AF and DF relaying in cooperative NOMA systems. In Proceedings of the 2019 19th International Conference on Sciences and Techniques of Automatic Control and Computer Engineering (STA), Sousse, Tunisia, 24–26 March 2019; pp. 614–619.

24. Gong, X.; Yue, X.; Liu, F. Performance analysis of cooperative NOMA networks with imperfect CSI over Nakagami-m fading channels. *Sensors* **2020**, *20*, 424.

25. Tran, D.D.; Ha, D.B.; So-In, C.; Tran, H.; Nguyen, T.G.; Baig, Z.A.; Sanguanpong, S. Performance Analysis of DF/AF Cooperative MISO Wireless Sensor Networks With NOMA and SWIPT Over Nakagami-*m* Fading. *IEEE Access* **2018**, *6*, 56142–56161.

26. Aldababsa, M.; Kucur, O. Performance of cooperative multiple-input multiple-output NOMA in Nakagami-m fading channels with channel estimation errors. *IET Commun.* **2020**, *14*, 274–281.

27. Nguyen, X.X.; Do, D.T. System performance of cooperative NOMA with full-duplex relay over Nakagami-m fading channels. *Mob. Inf. Syst.* **2019**, *2019*, 7547431.

28. Li, G.; Mishra, D. Cooperative NOMA networks: User cooperation or relay cooperation? In Proceedings of the ICC 2020—2020 IEEE International Conference on Communications (ICC), Dublin, Ireland, 7–11 June 2020; pp. 1–6.

29. Goutham, V.; Harigovindan, V. Full-duplex cooperative relaying with NOMA for the performance enhancement of underwater acoustic sensor networks. *Eng. Sci. Technol. Int. J.* **2021**, *24*, 1396–1407.

30. Kramer, G.; Maric, I.; Yates, R.D. *Cooperative Communications*; Now Publishers Inc.: Hanover, MA, USA 2007.

31. Zhou, Y.; Wong, V.W.; Schober, R. Performance analysis of cooperative NOMA with dynamic decode-and-forward relaying. In Proceedings of the GLOBECOM 2017—2017 IEEE Global Communications Conference, Singapore, 4–8 December 2017; pp. 1–6.

32. Umakoglu, I.; Namdar, M.; Basgumus, A.; Kara, F.; Kaya, H.; Yanikomeroglu, H. BER Performance Comparison of AF and DF Assisted Relay Selection Schemes in Cooperative NOMA Systems. In Proceedings of the 2021 IEEE International Black Sea Conference on Communications and Networking (BlackSeaCom), Bucharest, Romania, 24–28 May 2021; pp. 1–6.

33. Zheng, B.; Wen, M.; Wang, C.X.; Wang, X.; Chen, F.; Tang, J.; Ji, F. Secure NOMA based two-way relay networks using artificial noise and full duplex. *IEEE J. Sel. Areas Commun.* **2018**, *36*, 1426–1440.

34. Men, J.; Ge, J. Performance analysis of non-orthogonal multiple access in downlink cooperative network. *IET Commun.* **2015**, *9*, 2267–2273.

35. Abbasi, O.; Ebrahimi, A. Cooperative NOMA with full-duplex amplify-and-forward relaying. *Trans. Emerg. Telecommun. Technol.* **2018**, *29*, e3421.
36. Liang, X.; Wu, Y.; Ng, D.W.K.; Zuo, Y.; Jin, S.; Zhu, H. Outage performance for cooperative NOMA transmission with an AF relay. *IEEE Commun. Lett.* **2017**, *21*, 2428–2431.
37. Li, Y.; Kishore, S. Asymptotic analysis of amplify-and-forward relaying in Nakagami-fading environments. *IEEE Trans. Wirel. Commun.* **2007**, *6*, 4256–4262.
38. Peppas, K.P.; Alexandropoulos, G.C.; Mathiopoulos, P.T. Performance Analysis of Dual-Hop AF Relaying Systems over Mixed $\eta-\mu$ and $\kappa-\mu$ Fading Channels. *IEEE Trans. Veh. Technol.* **2013**, *62*, 3149–3163.
39. Kim, J.B.; Lee, I.H. Capacity analysis of cooperative relaying systems using non-orthogonal multiple access. *IEEE Commun. Lett.* **2015**, *19*, 1949–1952.
40. So, J.; Sung, Y. Improving non-orthogonal multiple access by forming relaying broadcast channels. *IEEE Commun. Lett.* **2016**, *20*, 1816–1819.
41. Liu, H.; Ding, Z.; Kim, K.J.; Kwak, K.S.; Poor, H.V. Decode-and-forward relaying for cooperative NOMA systems with direct links. *IEEE Trans. Wirel. Commun.* **2018**, *17*, 8077–8093.
42. Li, G.; Mishra, D.; Hu, Y.; Huang, Y.; Jiang, H. Adaptive Relay Selection Strategies for Cooperative NOMA Networks With User and Relay Cooperation. *IEEE Trans. Veh. Technol.* **2020**, *69*, 11728–11742.
43. Wu, X.; Xie, L.L. On the optimal compressions in the compress-and-forward relay schemes. *IEEE Trans. Inf. Theory* **2013**, *59*, 2613–2628.
44. Liaqat, M.; Noordin, K.A.; Latef, T.A.; Dimyati, K. Power-domain non orthogonal multiple access (PD-NOMA) in cooperative networks: An overview. *Wirel. Netw.* **2020**, *26*, 181–203.
45. Zeng, M.; Hao, W.; Dobre, O.A.; Ding, Z. Cooperative NOMA: State of the Art, Key Techniques, and Open Challenges. *IEEE Netw.* **2020**, *34*, 205–211.
46. Li, Y.; Li, Y.; Chu, X.; Ye, Y.; Zhang, H. Performance analysis of relay selection in cooperative NOMA networks. *IEEE Commun. Lett.* **2019**, *23*, 760–763.
47. Kaur, J.; Singh, M.L. User assisted cooperative relaying in beamspace massive MIMO NOMA based systems for millimeter wave communications. *China Commun.* **2019**, *16*, 103–113.
48. Sushma, J.; Gayathri, M.N.; Srivani, S.; Nayak, V.N.; Gurrala, K.K. Performance Analysis and Power allocation for Multi Relay Wireless Cooperative NOMA Networks with Diversity Combining strategies. In Proceedings of the 2020 IEEE International Students' Conference on Electrical, Electronics and Computer Science (SCEECS), Bhopal, India, 22–23 February 2020; pp. 1–6.
49. Mohammadi, M.; Shi, X.; Chalise, B.K.; Ding, Z.; Suraweera, H.A.; Zhong, C.; Thompson, J.S. Full-duplex non-orthogonal multiple access for next generation wireless systems. *IEEE Commun. Mag.* **2019**, *57*, 110–116.
50. Zhang, Z.; Si, Z. Performance Evaluation and Optimization of Cooperative NOMA over Rayleigh Fading Channels. In Proceedings of the 2020 IEEE International Conference on Communications Workshops (ICC Workshops), Dublin, Ireland, 7–11 June 2020; pp. 1–6.
51. Wang, H.; Shi, R.; Tang, K.; Dong, J.; Liao, S. Performance Analysis and Optimization of a Cooperative Transmission Protocol in NOMA-Assisted Cognitive Radio Networks with Discrete Energy Harvesting. *Entropy* **2021**, *23*, 785.
52. Alnwaimi, G.; Boujemaa, H.; Arshad, K. Throughput optimization of cooperative non orthogonal multiple access. *Telecommun. Syst.* **2021**, *76*, 359–370.
53. Ali, Z.; Khan, W.U.; Ihsan, A.; Waqar, O.; Sidhu, G.A.S.; Kumar, N. Optimizing Resource Allocation for 6G NOMA-enabled Cooperative Vehicular Networks. *IEEE Open J. Intell. Transp. Syst.* **2021**, *2*, 269–281.
54. Reshma, K.; Babu, A. Cooperative NOMA system with incremental relaying and energy harvesting: Performance analysis and optimization. *Trans. Emerg. Telecommun. Technol.* **2020**, *31*, e4075.
55. Nazari, A.; Javan, M.R.; Hosseini, S.S. Resource allocation in power domain NOMA-based cooperative multicell networks. *IET Commun.* **2020**, *14*, 1162–1168.
56. Li, J.; Lei, X.; Diamantoulakis, P.D.; Zhou, F.; Sarigiannidis, P.; Karagiannidis, G.K. Resource allocation in buffer-aided cooperative non-orthogonal multiple access systems. *IEEE Trans. Commun.* **2020**, *68*, 7429–7445.
57. Wang, L.; Xu, D. Resource allocation in downlink SWIPT-based cooperative NOMA systems. *KSII Trans. Internet Inf. Syst. (TIIS)* **2020**, *14*, 20–39.
58. Chen, X.; Wen, M.; Mao, T.; Dang, S. Spectrum resource allocation based on cooperative NOMA with index modulation. *IEEE Trans. Cogn. Commun. Netw.* **2020**, *6*, 946–958.
59. Rezaei, A.; Azmi, P.; Yamchi, N.M.; Javan, M.R.; Yanikomeroglu, H. Robust Resource Allocation for Cooperative MISO-NOMA-Based Heterogeneous Networks. *IEEE Trans. Commun.* **2021**, *69*, 3864–3878.
60. Amer, A.; Ahmad, A.M.; Hoteit, S. Resource allocation for downlink full-duplex cooperative NOMA-based cellular system with imperfect SI cancellation and underlaying D2D communications. *Sensors* **2021**, *21*, 2768.
61. Chen, X.; Jia, R.; Ng, D.W.K. The application of relay to massive non-orthogonal multiple access. *IEEE Trans. Commun.* **2018**, *66*, 5168–5180.
62. Abolpour, M.; Mirmohseni, M.; Aref, M.R. Outage performance in secure cooperative NOMA. In Proceedings of the 2019 Iran Workshop on Communication and Information Theory (IWCIT), Tehran, Iran, 24–25 April 2019; pp. 1–6.

63. Zhang, J.; Tao, X.; Wu, H.; Zhang, X. Performance analysis of user pairing in cooperative NOMA networks. *IEEE Access* **2018**, *6*, 74288–74302.

64. Zhou, Y.; Wong, V.W.; Schober, R. Dynamic decode-and-forward based cooperative NOMA with spatially random users. *IEEE Trans. Wirel. Commun.* **2018**, *17*, 3340–3356.

65. Zhou, T.; Yang, Y.; Liu, L.; Tao, C.; Liang, Y. A Dynamic 3-D Wideband GBSM for Cooperative Massive MIMO Channels in Intelligent High-Speed Railway Communication Systems. *IEEE Trans. Wirel. Commun.* **2020**, *20*, 2237–2250.

66. Hong, Y.W.P.; Huang, W.J.; Kuo, C.C.J. *Cooperative Communications and Networking: Technologies and System Design*; Springer Science & Business Media: New York, USA 2010; Chapter 1, pp. 1–10.

67. Huang, H.; Zhu, M. Energy efficiency maximization design for full-duplex cooperative NOMA systems with SWIPT. *IEEE Access* **2019**, *7*, 20442–20451.

68. Liu, K.R.; Sadek, A.K.; Su, W.; Kwasinski, A. *Cooperative Communications and Networking*; Cambridge University Press: Cambridge, UK, 2009.

69. Elouafadi, R.; Benjillali, M. Cooperative NOMA-based D2D communications: A survey in the 5G/IoT context. In Proceedings of the 2018 19th IEEE Mediterranean Electrotechnical Conference (MELECON), Marrakech, Morocco, 2–7 May 2018; pp. 132–137.

70. Abbasi, O.; Ebrahimi, A.; Mokari, N. NOMA inspired cooperative relaying system using an AF relay. *IEEE Wirel. Commun. Lett.* **2018**, *8*, 261–264.

71. Abdel-Razeq, S.; Zhou, S.; Bansal, R.; Zhao, M. Uplink NOMA transmissions in a cooperative relay network based on statistical channel state information. *IET Commun.* **2019**, *13*, 371–378.

72. Huang, Y.; Zhang, C.; Wang, J.; Jing, Y.; Yang, L.; You, X. Signal processing for MIMO-NOMA: Present and future challenges. *IEEE Wirel. Commun.* **2018**, *25*, 32–38.

73. Aldababsa, M.; Kucur, O. Outage and ergodic sum-rate performance of cooperative MIMO-NOMA with imperfect CSI and SIC. *Int. J. Commun. Syst.* **2020**, *33*, e4405.

74. Singh, S.; Bansal, M. Outage analysis of NOMA-based cooperative relay systems with imperfect SIC. *Phys. Commun.* **2020**, *43*, 101219. https://doi.org/10.1016/j.phycom.2020.101219.

75. Belmekki, B.E.Y.; Hamza, A.; Escrig, B. On the performance of cooperative NOMA Using MRC at road intersections in the presence of interference. *Phys. Commun.* **2021**, *46*, 101321. https://doi.org/10.1016/j.phycom.2021.101321.

76. Chen, X.; Gong, F.K.; Li, G.; Zhang, H.; Song, P. User pairing and pair scheduling in massive MIMO-NOMA systems. *IEEE Commun. Lett.* **2017**, *22*, 788–791.

77. Ding, Z.; Dai, H.; Poor, H.V. Relay selection for cooperative NOMA. *IEEE Wirel. Commun. Lett.* **2016**, *5*, 416–419.

78. Men, J.; Ge, J. Non-orthogonal multiple access for multiple-antenna relaying networks. *IEEE Commun. Lett.* **2015**, *19*, 1686–1689.

79. Nasir, H.; Javaid, N.; Raza, W. Study of buffer-aided cooperative NOMA using incremental relaying in wireless networks. *Phys. Commun.* **2020**, *39*, 101011.

80. Jiao, R.; Dai, L.; Zhang, J.; MacKenzie, R.; Hao, M. On the performance of NOMA-based cooperative relaying systems over Rician fading channels. *IEEE Trans. Veh. Technol.* **2017**, *66*, 11409–11413.

81. Fang, Z.; Hu, J.; Lu, Y.; Ni, W. Three-User Cooperative NOMA Transmission. *IEEE Wirel. Commun. Lett.* **2019**, *9*, 465–469.

82. Ju, J.; Duan, W.; Sun, Q.; Gao, S.; Zhang, G. Performance analysis for cooperative NOMA with opportunistic relay selection. *IEEE Access* **2019**, *7*, 131488–131500.

83. Lv, L.; Ye, Q.; Ding, Z.; Li, Z.; Al-Dhahir, N.; Chen, J. Multi-antenna two-way relay based cooperative NOMA. *IEEE Trans. Wirel. Commun.* **2020**, *19*, 6486–6503.

84. Cao, Y.; Zhao, N.; Pan, G.; Chen, Y.; Fan, L.; Jin, M.; Alouini, M.S. Secrecy analysis for cooperative NOMA networks with multi-antenna full-duplex relay. *IEEE Trans. Commun.* **2019**, *67*, 5574–5587.

85. Salem, A.; Musavian, L. NOMA in cooperative communication systems with energy-harvesting nodes and wireless secure transmission. *IEEE Trans. Wirel. Commun.* **2020**, *20*, 1023–1037.

86. Alkhawatrah, M.; Gong, Y.; Chen, G.; Lambotharan, S.; Chambers, J.A. Buffer-aided relay selection for cooperative NOMA in the Internet of Things. *IEEE Internet Things J.* **2019**, *6*, 5722–5731.

87. Mei, W.; Zhang, R. Uplink cooperative NOMA for cellular-connected UAV. *IEEE J. Sel. Top. Signal Process.* **2019**, *13*, 644–656.

88. Liau, Q.Y.; Leow, C.Y. Successive user relaying in cooperative NOMA system. *IEEE Wirel. Commun. Lett.* **2019**, *8*, 921–924.

89. Imoize, A.L.; Ibhaze, A.E.; Atayero, A.A.; Kavitha, K. Standard Propagation Channel Models for MIMO Communication Systems. *Wirel. Commun. Mob. Comput.* **2021**, *2021*, 8838792.

90. Meredith, J. Study on Channel Model for Frequency Spectrum above 6 GHZ. 3GPP TR 38.900 Jun Technical Report. 2016. Available online: https://portal.3gpp.org/desktopmodules/Specifications/SpecificationDetails.aspx?specificationId=2991 (accessed on: 20 February 2021).

91. Mondal, B.; Thomas, T.A.; Visotsky, E.; Vook, F.W.; Ghosh, A.; Nam, Y.H.; Li, Y.; Zhang, J.; Zhang, M.; Luo, Q.; et al. 3D channel model in 3GPP. *IEEE Commun. Mag.* **2015**, *53*, 16–23.

92. Nadeem, Q.U.A.; Kammoun, A.; Debbah, M.; Alouini, M.S. Spatial correlation characterization of a uniform circular array in 3D MIMO systems. In Proceedings of the 2016 IEEE 17th International Workshop on Signal Processing Advances in Wireless Communications (SPAWC), Edinburgh, UK, 3–6 July 2016; pp. 1–6. https://doi.org/10.1109/SPAWC.2016.7536796.

93. Assiimwe, E.; Marye, Y.W. A Stochastic Confocal Elliptic-Cylinder Channel Model for 3D MIMO in Millimeter-Wave High-Speed Train Communication System. *Electronics* **2022**, *11*, 1948. https://doi.org/10.3390/electronics11131948.

94. Ahmed, N.; Hua, B.; Zhu, Q.; Mao, K.; Bao, J. A Novel GBSM for Non-Stationary V2V Channels Allowing 3D Velocity Variations. *Sensors* **2021**, *21*, 3271. https://doi.org/10.3390/s21093271.

95. Kammoun, A.; Debbah, M.; Alouini, M.S. 3D massive MIMO systems: Modeling and performance analysis. *IEEE Trans. Wirel. Commun.* **2015**, *14*, 6926–6939.

96. May Taniguchi, L.; Abrao, T. Stochastic channel models for massive and extreme large multiple-input multiple-output systems. *Trans. Emerg. Telecommun. Technol.* **2020**, *31*, e4099.

97. Yuan, Y.; He, R.; Ai, B.; Ma, Z.; Miao, Y.; Niu, Y.; Zhang, J.; Chen, R.; Zhong, Z. A 3D Geometry-Based THz Channel Model for 6G Ultra Massive MIMO Systems. *IEEE Trans. Veh. Technol.* **2022**, *71*, 2251–2266.

98. Björnson, E.; Hoydis, J.; Kountouris, M.; Debbah, M. Massive MIMO systems with non-ideal hardware: Energy efficiency, estimation, and capacity limits. *IEEE Trans. Inf. Theory* **2014**, *60*, 7112–7139.

99. Salo, J. Universal mobile telecommunications system (UMTS); Spatial channel model for multiple input multiple output (MIMO) simulations. Eur. Telecommun. Standards Inst., Nice, French, Technical Report GT. 2020; Volume 25. Available online: https://portal.3gpp.org/desktopmodules/Specifications/SpecificationDetails.aspx?specificationId=1382 (accessed on: 10 February 2021).

100. Guan, K.; He, D.; Ai, B.; Chen, Y.; Han, C.; Peng, B.; Zhong, Z.; Kuerner, T. Channel characterization and capacity analysis for THz communication enabled smart rail mobility. *IEEE Trans. Veh. Technol.* **2021**, *70*, 4065–4080.

101. Guan, K.; Ai, B.; He, D.; Zhu, F.; Yi, H.; Dou, J.; Zhong, Z. Channel sounding and ray tracing for thz channel characterization. In Proceedings of the 2020 13th UK-Europe-China Workshop on Millimetre-Waves and Terahertz Technologies (UCMMT), Tianjin, China, 29 August–1 September 2020; pp. 1–3.

102. Yong, S.K.; Thompson, J.S. Three-dimensional spatial fading correlation models for compact MIMO receivers. *IEEE Trans. Wirel. Commun.* **2005**, *4*, 2856–2869.

103. Ademaj, F.; Taranetz, M.; Rupp, M. 3GPP 3D MIMO channel model: A holistic implementation guideline for open source simulation tools. *EURASIP J. Wirel. Commun. Netw.* **2016**, *2016*, 1–14.

104. Zeng, L.; Cheng, X.; Wang, C.X.; Yin, X. A 3D geometry-based stochastic channel model for UAV-MIMO channels. In Proceedings of the 2017 IEEE Wireless Communications and Networking Conference (WCNC), San Francisco, CA, USA, 19–22 March 2017; pp. 1–5.

105. Zheng, Y.; Yu, L.; Yang, R.; Wang, C.X. A General 3D Non-Stationary Massive MIMO GBSM for 6G Communication Systems. In Proceedings of the 2021 IEEE Wireless Communications and Networking Conference (WCNC), Nanjing, China, 29 March–1 April 2021; pp. 1–6.

106. Zeng, W.; He, Y.; Li, B.; Wang, S. 3D Multiple-Antenna Channel Modeling and Propagation Characteristics Analysis for Mobile Internet of Things. *Sensors* **2021**, *21*, 989.

107. Bello, O.; Zen, H.; Othman, A.K.; Hamid, K.A. Computing amplify-and-forward relay amplification factor to improve total capacity at destination. *Am. J. Appl. Sci.* **2015**, *12*, 572.

108. Dai, L.; Wang, B.; Yuan, Y.; Han, S.; Chih-Lin, I.; Wang, Z. Non-orthogonal multiple access for 5G: Solutions, challenges, opportunities, and future research trends. *IEEE Commun. Mag.* **2015**, *53*, 74–81.

109. Wang, Z.; Peng, Z.; Pei, Y.; Wang, H. Performance Analysis of Cooperative NOMA Systems with Incremental Relaying. *Wirel. Commun. Mob. Comput.* **2020**, *2020*, 4915638.

110. Blahut, R.E. 25—Information Theory and Coding. In *Reference Data for Engineers*, 9th ed.; Middleton, W.M., Van Valkenburg, M.E., Eds.; Newnes: Woburn, MA, USA, 2002; pp. 25-1–25-31. https://doi.org/10.1016/B978-075067291-7/50027-3.

111. Kara, F.; Kaya, H. BER performances of downlink and uplink NOMA in the presence of SIC errors over fading channels. *IET Commun.* **2018**, *12*, 1834–1844.

112. Shen, M.; Huang, Z.; Lei, X.; Fan, L. BER analysis of NOMA with max-min relay selection. *China Commun.* **2021**, *18*, 172–182.

113. Ampoma, A.E.; Zhang, H.; Huang, Y.; Wen, G.; Kwame, O.G. On massive MIMO antenna topologies using total power in the azimuth and zenith domains. In Proceedings of the 2017 IEEE International Symposium on Antennas and Propagation & USNC/URSI National Radio Science Meeting, San Diego, CA, USA, 9–14 July 2017; pp. 369–370.

114. Su, J.; Shen, J.; Liu, W.; Guo, L. Chapter 1 - Overview. In *5G NR and Enhancements*; Shen, J., Du, Z., Zhang, Z., Yang, N., Tang, H., Eds.; Elsevier: Amsterdam, The Netherlands, 2022; pp. 1–39. https://doi.org/10.1016/B978-0-323-91060-6.00001-5.

115. Ropokis, G.A.; Rontogiannis, A.A.; Berberidis, K. BER performance analysis of cooperative DaF relay networks and a new optimal DaF strategy. *IEEE Trans. Wirel. Commun.* **2011**, *10*, 1044–1049.

116. Li, Q.; Wen, M.; Basar, E.; Poor, H.V.; Chen, F. Spatial modulation-aided cooperative NOMA: Performance analysis and comparative study. *IEEE J. Sel. Top. Signal Process.* **2019**, *13*, 715–728.

117. Yang, Z.; Ding, Z.; Wu, Y.; Fan, P. Novel relay selection strategies for cooperative NOMA. *IEEE Trans. Veh. Technol.* **2017**, *66*, 10114–10123.

118. Hoang, T.M.; Nguyen, B.C.; Tran, X.N.; Dung, L.T. Outage Probability and Ergodic Capacity of User Clustering and Beamforming MIMO-NOMA Relay System With Imperfect CSI Over Nakagami-*m* Fading Channels. *IEEE Syst. J.* **2020**, *15*, 2398–2409. https://doi.org/10.1109/JSYST.2020.3009700.

119. Le, C.B.; Do, D.T.; Voznak, M. Wireless-powered cooperative MIMO NOMA networks: Design and performance improvement for cell-edge users. *Electronics* **2019**, *8*, 328.